BRILL

*Seeing and Perceiving 23 (2010) 223–240*

brill.nl/sp

# The Munker–White Effect and Chromatic Induction Share Similar Nonlinear Response Properties

**Yong-Jun Lin** [1], **Chien-Chung Chen** [1,*] **and Sarina Hui-Lin Chien** [1,2]

[1] Department of Psychology, National Taiwan University, Taipei, Taiwan

[2] Graduate Institute of Neural and Cognitive Sciences, China Medical University, Taichung, Taiwan

Received 13 August 2009; accepted 3 May 2010

**Abstract**

The brightness or color appearance of a region may be altered by the presence of a pattern surrounding it in the visual field. The Munker–White effect (grating surround) and brightness or color induction from concentric annuli ('bull's-eye' surround) are two examples. We examined whether these two phenomena share similar properties. In the asymmetric matching experiment, the task of an observer was to adjust the appearance of a matching patch to match the appearance of a test patch embedded in one of the two types (square wave grating or concentric annuli) of inducing surrounds (inducers). The inducer modulated in one of three color directions (isochromatic: $\pm(L + M + S)$ and isoluminance: $\pm(L - M)$ or $\pm S$). Each inducer type and color direction had two opposing phases and four contrast levels. The results show that the induced appearance shift increases as a power function of the inducer contrast, regardless of the spatial configuration of the inducer. Further analysis showed that a sensitivity modulation model of lateral interaction could explain both induction effects.



**Keywords**

Brightness, asymmetric matching, contrast appearance, pattern

## 1. Introduction

The brightness and the color appearance of a uniform patch can be affected by a patterned surround. Munker (1970) demonstrated such effects by embedding a short bar in a square-wave grating alternating in two colors (Fig. 1(a)). He showed that a red bar appeared yellowish when placed on a blue stripe of a yellow/blue square-wave grating, while the same red bar appeared bluish when placed on a yellow stripe of the same grating. Similar color appearance shifts were observed with other color combinations. White (1979) reported a similar effect with brightness shift

* To whom correspondence should be addressed. E-mail: c3chen@ntu.edu.tw



DOI:10.1163/187847510X516395

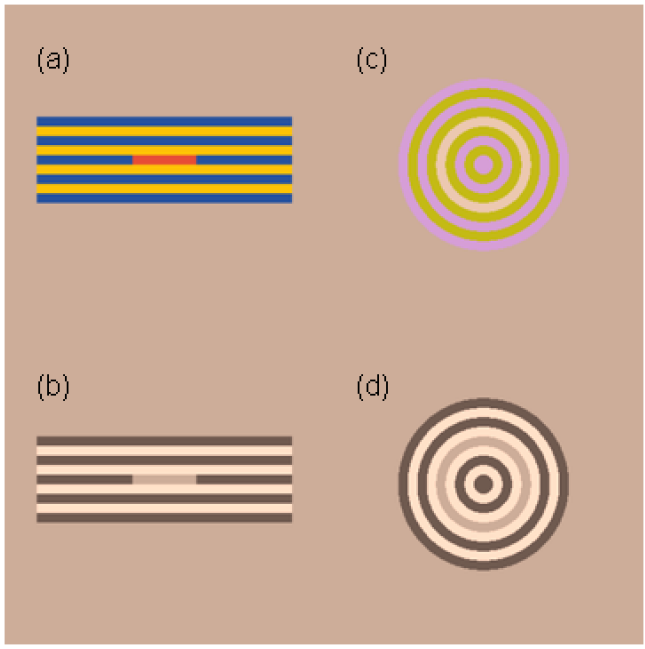


**Figure 1.** (a) The Munker effect (Munker, 1970): color shift induced by bi-color grating. (b) The White effect (White, 1979): brightness shift induced by bi-color grating. (c) Monnier and Shevell (2003): *S*-cone color shift induced by bi-color concentric annuli. (d) Hong and Shevell (2004): brightness shift induced by bi-color concentric annuli. See text for description. This figure is published in colour online, see http://www.brill.nl/sp

(Fig. 1(b)). He showed that a gray bar placed on a white stripe of a black-and-white square-wave grating surround appeared darker than the same gray bar on a black stripe of the same grating. Since the spatial configurations of Munker's and White's stimuli are both rectangular gratings, in this paper we followed the same convention used in the literature (Taya *et al.*, 1995) and call both effects *the Munker–White effect*.

Likewise, similar appearance shifts can be induced by surrounds with a different spatial configuration. Using square-wave concentric annuli surround modulated in purple (*S*-cone response increment) and yellow (*S*-cone response decrement), Monnier and Shevell (2003) demonstrated that a gray ring replacing a purple ring of the concentric annuli pattern appeared yellowish, while a gray ring replacing a yellow ring of the concentric annuli pattern would appear purplish (Fig. 1(c)). Hong and Shevell (2004) also demonstrated a brightness shift with an isochromatic version of the same display (Fig. 1(d)). For the convenience of discussion, we will call this appearance shift induced by a concentric surround the *annulus pattern induction effect*.

One particular study has adopted both configurations in the brightness (or luminance) domain; Howe (2005) demonstrated that a similar induction effect was observed with the Munker–White and the annulus configurations. While Howe

(2005) did not mention the annulus pattern induction effect, the annulus stimuli used in that paper were almost identical to those Hong and Shevell (2004) used. This result suggests that a common mechanism may mediate both the Munker–White effect and the annulus pattern induction effect. If it can be proven that the induction effects from these two very diverse spatial configurations were related, this would have a significant theoretical implication on the nature of the inductions. We will discuss this later in the paper.

Since most annulus color induction studies used only chromaticity modulating in *S*-cone excitation, how general the phenomenon is remains in question. Therefore, the goals of the present study were threefold. First, we are interested in testing whether this effect can be observed with chromaticity in $L - M$ cone excitation, that is, along another cardinal axis. Second, we asked whether the result of Howe (2005) can be expanded to color induction effects. After all, it is known that the spatiotemporal characteristics of luminance and color processing are quite different. For instance, the contrast sensitivity functions for luminance stimuli are band-pass (Carney *et al.*, 2000; Kelly, 1983; Robson, 1966), whereas those for isoluminant stimuli are low-pass (Kelly, 1983; Mullen, 1985). The results acquired with luminance stimuli may not be the same as those acquired with isoluminant stimuli.

Third, we are interested in the contrast response characteristics of the mechanisms underlying these induction effects, that is, how the response of the underlying mechanisms changed with inducing contrast. In a detection paradigm, such information is obtained by detecting a target superimposed on pedestals that are systematically varied in contrast (Chen and Tyler, 2001; Foley, 1994; Legge and Foley, 1980). Here, we used an asymmetric matching paradigm to measure the magnitude of the induced effect as a function of inducing contrast. To the best of our knowledge, such information was not available for the Munker–White effect and was available for the annulus pattern induction effect only at *S*-cone modulation (Shevell and Monnier, 2005). Finally, we proposed a model for the lateral effect on pattern detection to best explain both the Munker–White and the annulus pattern induction effects.

## 2. Method

### 2.1. Apparatus

The stimuli were presented on a ViewSonic P75f+ 17″ CRT monitor controlled by a Macintosh G4 computer with an ATI Radeon 7500 graphics card with 10-bit color depth. The spatial resolution was 800 (H) × 600 (V). The viewing distance was 110 cm. At this distance, a pixel subtended about 0.02° (H) × 0.02° (V), and the whole display subtended 16.7° (H) × 12.5° (V). The temporal refresh rate of the monitor was 75 Hz (non-interlaced). The gamma function of the monitor was calibrated with a LightMouse photometer (Tyler and McBride, 1997), and this information was used to compute linear 10-bit color look-up tables for each contrast level and each chromatic condition tested. The accuracy of the color look-up ta-

bles was verified by an International Light RPS-380 spectroradiometer before and after the experiment. The experimental control software was written in MATLAB (MathWorks, 1993) with the Psychophysics Toolbox (Brainard, 1997; Pelli, 1997). A chin rest restrained the head position of the observers. The display had a mean luminance of 15 cd/m$^2$ and a mean chromaticity at (0.33, 0.33) in CIE 1931-$xy$ coordinates.

### 2.2. Stimuli

In each trial, the display contained an inducing pattern on one side of the screen and a matching pattern on the other side. The center of both patterns was 4.1° from the center of the screen. A binary random number generator determined whether the inducing pattern was on the left or the right side of the display.

An inducing pattern contained an inducer and a gray test patch. Two types of inducers were used (Fig. 2(a) and 2(b): the grating inducer for the Munker–White effect (Munker, 1970; White, 1979) and the concentric annuli inducer for annu-

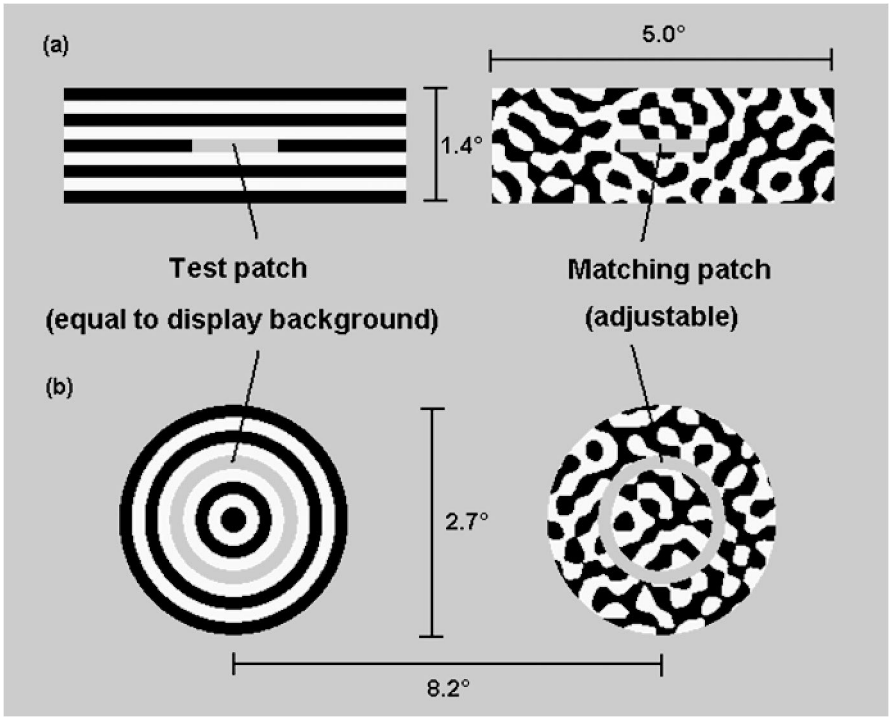


**Figure 2.** An illustration of the stimuli used in this study. In the left column are the two types of inducers. In the right column are the two types of matching surrounds. When the surrounds were modulated in a color direction, the induced appearance was also measured along that direction. (a) $A + (L + M + S)$ (see text for the definition of chromatic condition) grating inducer comparing to a scrambled matching surround. (b) $A + (L + M + S)$ concentric annuli inducer comparing to a scrambled matching surround.

lus pattern induction (Hong and Shevell, 2004; Monnier and Shevell, 2003). The grating inducer was a horizontally oriented square wave with a spatial frequency of 3.3 cycles per degree and a width of 4.5 cycles. Its size was 4.08° (H) × 1.36° (V). The test patch (0.82° H × 0.15° V) was a gray bar of mean luminance and chromaticity replaced part of the central stripe of the grating. Thus, two complete cycles of inducer were below and above the test patch.

The concentric annuli inducer was a concentric square wave with a spatial frequency of 3.3 cycles per degree, a radius of 4.5 cycles, and a size of 2.73° (H) × 2.73° (V). The test patch embedded in a concentric inducer was in a ring and replaced the fifth ring from the center of the inducer. Thus, two complete cycles, or four rings, appeared on either the inward or outward side of the inducer. The test patch always had the same chromaticity and luminance as the background in all conditions.

The matching pattern contained a matching patch embedded in a scrambled surround. The matching patch, the contrast of which could be adjusted by the observers, was either a bar or an annulus that had the same spatial properties as the corresponding test patch in the inducers. The scrambled surround had the same peak spatial frequency as the concentric inducer in its power spectrum, but had a scrambled phase spectrum. The luminance threshold of the scrambled surrounds was set at the median luminance to create the binary patterns used in the experiment.

The inducers were modulated either in luminance or in chromaticity. In the experiment, one isochromatic ($\pm(L+M+S)$) and two isoluminant ($\pm(L-M)$ and $\pm S$) modulations were used. Since the test patch could be superimposed on either the stripes or the rings of the inducers, there were two types of stimuli for each modulation axis. We thus named the inducers by the stripe or ring directly flanking the test patch on the wide side. That is, there were $+(L+M+S)$, $-(L+M+S)$, $+(L-M)$, $-(L-M)$, $+S$ and $-S$ inducing conditions. The names of these conditions indicated the induced chromaticity that was expected to be observed in each condition. The nominal excitation of each cone type ($L$, $M$ and $S$) to each incident light was computed as an inner product of the spectral power distribution of the light and the corresponding Smith–Pokorny cone fundamental (DeMarco *et al.*, 1992; Smith and Pokorny, 1975). Each sensitivity function was normalized such that the maximum sensitivity of each cone type was one. The chromaticity of the background, which had CIE-$xyY$ 1931 coordinates as $(0.33, 0.33, 15)$, had cone excitation $[L_0 \;\; M_0 \;\; S_0] = [0.023 \;\; 0.019 \;\; 0.012]$. The chromaticity of the stimuli was defined in cone contrast, which was a three-dimensional vector as $C = [C_L \;\; C_M \;\; C_S] = [\Delta L/L_0 \;\; \Delta M/M_0 \;\; \Delta S/S_0]$, where $L_0$, $M_0$ and $S_0$ are the $L$-, $M$- and $S$-cone excitation to the background, respectively, and $\Delta L$, $\Delta M$ and $\Delta S$ are the deviation of $L$-, $M$- and $S$-cone excitation to a stripe of the inducer or to the test patch from background. The term 'contrast' referred to the modulation against the background, not the difference between neighboring image components. The technical detail for specifying chromatic modulation of the stimuli was discussed elsewhere (Chen *et al.*, 2000a).

The chromaticity of each stimulus was specified by a normalized contrast vector, $C/\|C\|$, and the pooled contrast. The pooled contrast was the length of the cone contrast vector $c = (C_L^2 + C_M^2 + C_S^2)^{0.5}/3^{0.5}$. The range of $c$ was between 0 and 1. In this paper, unless otherwise mentioned, we specified the contrast in dB units, which is 20 times $\log_{10}(c)$. The isochromatic modulations had the same chromaticity as the background and thus had a normalized contrast vector: [0.577 0.577 0.577] for $+(L+M+S)$ and [−0.577 −0.577 −0.577] for $-(L+M+S)$, respectively. The isolumiance modulations were on the null plane of the Judd–Vos modified luminosity ($V_\lambda$ function (Vos, 1978)). Two pairs of nominal isoluminant chromaticity modulations ($M$-, $L$- and $S$-cone modulations) were used for inducers: [−0.452 0.892 0.000] and [0.452 −0.892 0.000] for $-(L-M)$ and $+(L-M)$, respectively, and [0.000 0.000 1.000] and [0.000 0.000 −1.000] for $+S$ and $-S$, respectively. There were also subjective isoluminant chromatic conditions near these axes determined for each individual observer using minimum motion technique (Anstis and Cavanagh, 1983).

Each inducer had four contrast levels for each chromaticity modulation. The ranges of the contrast levels were determined both by the measured detection thresholds for Gabor patterns obtained from previous studies (Chen *et al.*, 2000a) and by the maximum contrast that can be produced by our apparatus. The contrast range for the $\pm(L+M+S)$ isochromatic inducer was from −15 to −3 dB. The contrast ranges for the nominal isoluminant $\pm(L-M)$, $\pm S$, and the subjective isoluminant $\pm(L-M)$, $\pm S$ inducers were −31 to −19 dB, −19 to −7 dB, −27 to −19 dB, and −16 to −8 dB, respectively. The scrambled matching surround had the same contrast as the corresponding inducer.

### 2.3. Procedures

We used an asymmetric matching task to measure the induced brightness and color shifts. The observer's task was to adjust the appearance of the matching patch within the matching surround to match the appearance of the test patch within the inducer. The observers increased or decreased the contrast of the matching patch along the designated color direction by pressing one of the two buttons. A third button was pressed to signal that a match was achieved. The contrast increased or decreased by 0.5 dB for each step. The minimum contrast that can be correctly displayed on our apparatus was −37.5 dB for the isochromatic conditions and −51 to −49 dB (depended on the subjective isoluminance setting of each observer) for the $+(L-M)$ and $-(L-M)$ conditions. Measurements below these limits were considered as having no measurable effect and thus were excluded from the final data set. The initial contrast of the matching patch was randomized. Each condition was repeated 10 times. The order of experimental conditions and repetitions were completely randomized.

Six observers (O1, O2 and O3 are males, and O4, O5 and O6 are females, all in their early twenties) participated in this study. All had corrected-to-normal visual acuity (20/20). None of the observers showed deficit in color vision as screened by

Ishihara color plates. Informed consent was obtained from each observer before the experiment. Observer O1 was an author of this paper, and the rest were paid naïve observers. All observers completed a two-hour practice session before the formal experimental sessions. Observers O1 and O2 participated in the achromatic and the nominal isoluminant conditions. Observer O3 participated only in the nominal $\pm S$ conditions. To control for possible residual luminance artifact in the nominal isoluminant stimuli, we used minimum motion technique to determine the subjective isoluminant colors near $\pm(L - M)$ and $\pm S$ modulations for observers O4, O5 and O6. These subjective isoluminance settings were then used to construct the tailored induction stimuli for the aforementioned observers.

## 3. Results

Figure 3 shows the asymmetric matching results with nominal isoluminance stimuli. The top two rows (Fig. 3(a–f)) show the results for the $-S$ and the $+S$ modulations, the middle two rows (Fig. 3(g–j)) the $-(L - M)$ and the $+(L - M)$ modulations, and the bottom two rows (Fig. 3(k–n)) the $-(L + M + S)$ and the $+(L + M + S)$ modulations. Each column represents the data from one observer. In each panel, matched contrasts are plotted as a function of surround contrast. The abscissa represents the surround contrast and the ordinate represents the magnitude of the induced contrast shift. The error bars represent $\pm 1$ standard error of means and are usually smaller than the symbols.

For the $-S$ inducer (top row), the appearance of the test patch shifted toward $-S$, regardless of whether the inducer was grating (closed squares in Fig. 3(a–c)) or concentric annuli (closed circles). The $+S$ inducer, on the other hand, produced a $+S$ shift in the test patch for both grating (open squares in Fig. 3(d–f)) and concentric (open circles) configuration. In each case, matched contrast increased linearly with surround contrast in log–log plots, and thus the data can be fitted with straight lines, the slopes of which depend only on the chromaticity of the inducer and not on the spatial configuration. The solid lines are the fits for the grating configuration, while the dotted lines are for the concentric configuration. The details of the curve fitting are discussed later in this paper.

The $-(L - M)$ inducer produced a $-(L - M)$ shift in the test patch for both inducer spatial configurations, while the $+(L - M)$ inducer produced a $+(L - M)$ shift in the test patch. The amount of shift, measured as matched contrast, again increased linearly with inducer contrast on log–log coordinates, and the slope of increment depended only on the chromaticity of the inducer and not on the spatial configuration. The $-(L + M + S)$ inducer decreased the brightness of the test patch, and the $+(L + M + S)$ inducer increased it. Likewise, the amount of shift increased with inducer contrast, and the slope of change depends only on the type of modulation and not on the spatial configuration.

The Munker–White effect was observed in all tested color modulations. We noted that Munker's (1970) demonstrations were not in isoluminance. Later, most

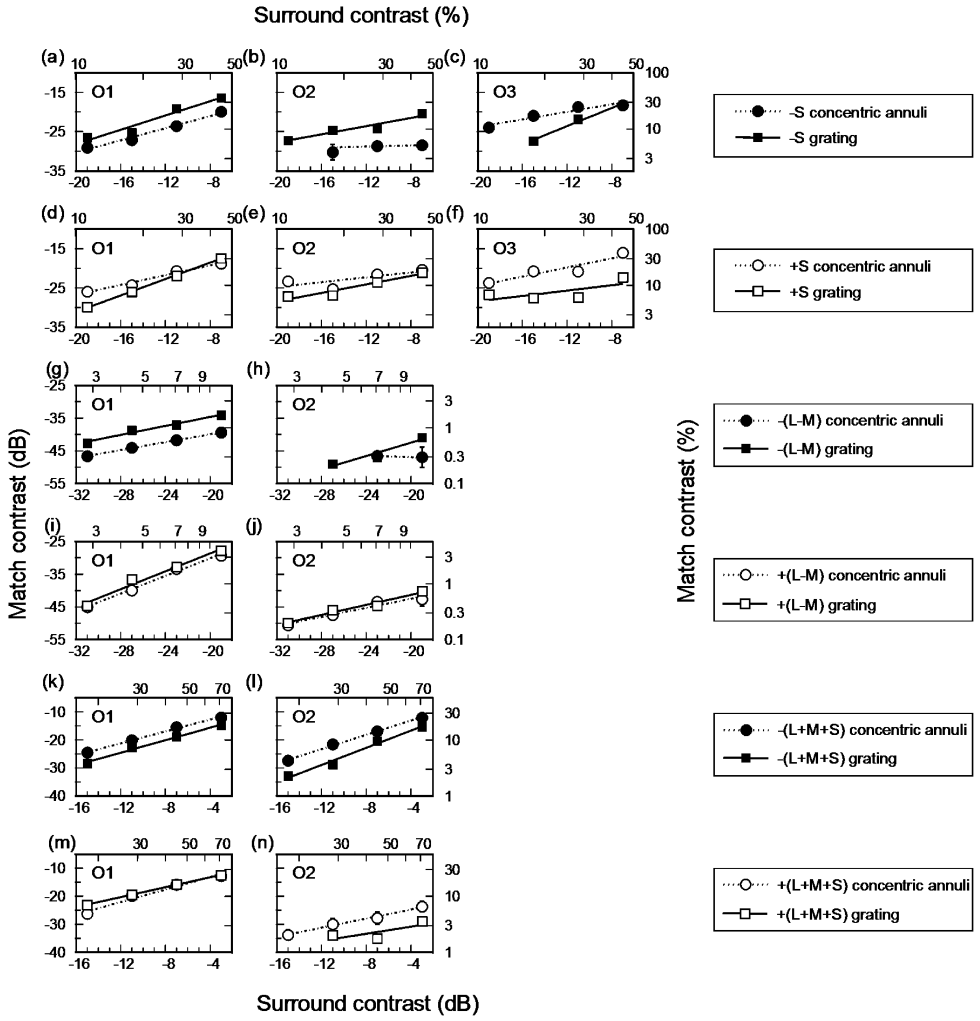


**Figure 3.** Asymmetric matching results with nominal isoluminance. All observers used the same stimulus setting. In each panel, matched contrast is plotted as a function of surround contrast on log–log scales. The abscissa represents the surround contrast, and the ordinate represents the magnitude of the induced contrast shift. From the top to the bottom row are the results in the $-S, +S, -(L-M), +(L-M), -(L+M+S)$ and $+(L+M+S)$ chromatic conditions, respectively. The results of different observers are shown in different column. In each chromatic condition, the chromaticity of the matches was also along that chromaticity. The induced appearance shifts by the grating and the concentric annuli have very similar trends in each chromatic condition.

Munker–White effect studies used stimuli modulated in luminance, yet we were able to get induced effect with the Munker–White configuration in all tested isoluminant color modulations.

While the nominal isoluminance conditions allowed the same test conditions for all observers and thus made a comparison across individuals possible, it may be ar-

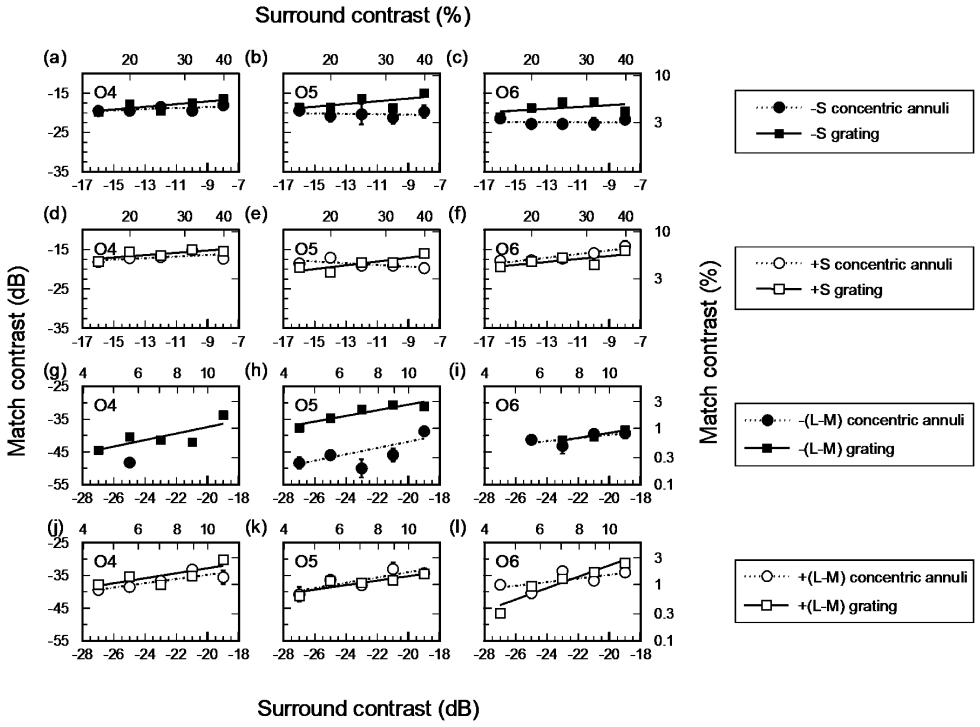


**Figure 4.** Asymmetric matching results with subjective isoluminance (stimuli were tailored to the isoluminance setting of each individual observer). The figure convention is the same as in Fig. 3, except that there are only $-S, +S, -(L-M)$ and $+(L-M)$ conditions. The induced appearance shifts have a similar trend for these two types of spatial configuration in each chromatic condition.

gued that the results of the nominal isoluminance conditions might be confounded by the residual luminance contrast in the stimuli. Hence, to control for this possible confounding variable, we repeated the experiment with the subjective isoluminance stimuli. Figure 4 shows the asymmetric matching results for the subjective isoluminance conditions. The result was basically the same as that for the nominal isoluminance data pattern shown in Fig. 3. Again, the slopes of the matching functions do not seem to depend on spatial configuration.

In Figs 3 and 4, note that certain matches with the lowest inducer contrasts were excluded because these matched values were below the measurable range of our apparatus. Thus, there was no measurable effect at these points.

## 4. Discussion

Overall, we showed that the appearance shift of the gray test patch induced by a grating surround was quite similar to that induced by a concentric annuli inducer. The appearance shift increased linearly with surround contrast in log–log coordinates, and the slope depended only on the chromatic modulation, and not on the

spatial configuration of the inducer. This implies that the mechanisms underlying the Munker–White effect and the annulus pattern induction effect share similar nonlinear properties.

### *4.1. The Power Function Relationship for the Induced Appearance Shift*

Since the background was constant throughout the experiment, all the effects measured in our experiment can be attributed to the modulation from the background. Thus, our analysis focused on the change of cone signal from the background, or cone contrast. As shown above, the data in each color direction and inducer phase appear to follow a linear trend on log–log plots. This implies that the matched contrast is likely to be described by a power function of surround contrast:

$$C_m = gC_s^h, \tag{1}$$

where $C_m$ is matched contrast, $C_s$ is surround contrast. Here, we tested the goodness-of-fit of power functions to the data. In our fits, the parameter $g$, which was related to sensitivity to the inducer (see below), was allowed to change for different spatial configurations, while the parameter $h$ was constrained to be the same for all spatial configurations of the same inducing chromatic modulation.

Table 1 shows the best-fitted parameters of this model for observers O1, O2 and O3 (nominal isoluminance), and observers O4, O5 and O6 (subjective isoluminance). The parameters $g_c$ and $g_s$ are the gain factors for the concentric annuli inducer and the stripe inducer, respectively. The parameters $h_c$ and $h_s$ are the power factors for the concentric annuli inducer and the stripe inducer, respectively. Each parameter has a best-fitted value for each chromatic condition (the combination of color directions and pattern phases).

This power function fit explains 88.9% of the total variability in the data. The root-mean-squared-error (RMSE) of the fit was 1.06 dB and was close to the mean standard error of measurements (1.01 dB). The fitted power parameters were significantly different from zero ($t(27) = 5.87$, $p < 0.0001$ for the nominal stimulus conditions and $t(21) = 5.50$, $p < 0.0001$ for the subjective stimulus conditions). This suggests that the induction effect increased with the inducer contrast. The fitted power parameters were also significantly different from one ($t(27) = 2.34$, $p < 0.05$ for the nominal stimulus conditions and $t(21) = 5.42$, $p < 0.0001$ for the subjective stimulus conditions). This shows that the induction effects with either annulus or grating inducers had a nonlinear property. To further test if a linear model could fit the data, we constrained the parameters $h_c$ and $h_s$ to be 1, that is, to reduce equation 1 to a linear function. Such a linear model could explain only 60.1% of the total variability in the data, and the RMSE was 2.01. The fit of this linear model was significantly worse than that of the nonlinear model ($F(51, 114) = 5.78$, $p < 0.0001$). Therefore, our result cannot be explained by a linear model. We also examined whether the power factors for the concentric annuli patterns and the grating patterns are different. A paired $t$-test showed that there was no significant difference in the power parameter for the two types of inducers ($t(13) = 1.98$, $p = 0.07$

**Table 1.**
Fitted parameters of the model

| Parameter | Chromatic condition | O1 | O2 | O3 | O4 | O5 | O6 |
|---|---|---|---|---|---|---|---|
| $g_c$ | $-S$ | 0.18 | 0.04 | 0.19 | 0.14 | 0.09 | 0.07 |
| | $+S$ | 0.19 | 0.12 | 0.23 | 0.18 | 0.09 | 0.28 |
| | $-(L-M)$ | 0.04 | 0.00 | | | 0.07 | 0.03 |
| | $+(L-M)$ | 0.68 | 0.04 | | 0.08 | 0.13 | 0.07 |
| | $-(L+M+S)$ | 0.37 | 0.39 | | | | |
| | $+(L+M+S)$ | 0.36 | 0.08 | | | | |
| $g_s$ | $-S$ | 0.32 | 0.14 | 0.32 | 0.20 | 0.22 | 0.16 |
| | $+S$ | 0.31 | 0.13 | 0.08 | 0.23 | 0.23 | 0.22 |
| | $-(L-M)$ | 0.09 | 0.08 | | 0.13 | 0.21 | 0.07 |
| | $+(L-M)$ | 0.84 | 0.05 | | 0.13 | 0.08 | 1.38 |
| | $-(L+M+S)$ | 0.27 | 0.29 | | | | |
| | $+(L+M+S)$ | 0.32 | 0.04 | | | | |
| $h_c$ | $-S$ | 0.77 | 0.07 | 0.48 | 0.14 | −0.05 | −0.02 |
| | $+S$ | 0.62 | 0.31 | 0.58 | 0.19 | −0.22 | 0.46 |
| | $-(L-M)$ | 0.60 | −0.10 | | | 0.97 | 0.48 |
| | $+(L-M)$ | 1.34 | 0.69 | | 0.65 | 0.81 | 0.56 |
| | $-(L+M+S)$ | 1.06 | 1.27 | | | | |
| | $+(L+M+S)$ | 1.11 | 0.81 | | | | |
| $h_s$ | $-S$ | 0.91 | 0.52 | 1.15 | 0.34 | 0.35 | 0.23 |
| | $+S$ | 1.04 | 0.54 | 0.34 | 0.29 | 0.48 | 0.38 |
| | $-(L-M)$ | 0.68 | 1.01 | | 0.99 | 0.86 | 0.78 |
| | $+(L-M)$ | 1.36 | 0.76 | | 0.77 | 0.69 | 1.74 |
| | $-(L+M+S)$ | 1.11 | 1.53 | | | | |
| | $+(L+M+S)$ | 0.88 | 0.63 | | | | |

for the nominal stimulus conditions and $t(9) = 2.05$, $p = 0.07$ for the subjective stimulus conditions).

### *4.2. The Power Function Relationship is Consistent with Long-Range Interactions between Oriented Mechanisms*

In this section, we show that the power function relationship may be due to the long-range interactions between oriented mechanisms. Researchers have shown (Chen and Tyler, 2001, 2002, 2008; Chen *et al.*, 2001) that the response of an oriented pattern mechanism to an image component in the presence of another image component has the form:

$$R_j = \left(Ke \cdot E_j^p\right)/(Ki \cdot I_j + Z), \tag{2}$$

where $R_j$ is the response of the $j$th mechanism; $E_j$ is the excitation of the $j$th linear filter, the receptive field of which overlaps with the target image element; $I_j$ is the divisive inhibition received by the $j$th mechanism; $Ke$ and $Ki$ are the excitatory and

inhibitory effects produced by the collinear lateral image components, respectively; $Z$ is the additive constant; and $p$ is the power factor of the excitatory signal. This model has successfully accounted for psychophysical and neurophysiological data (Chen and Tyler, 2001, 2002, 2008; Chen *et al.*, 2001). Similar formulation has been applied to explain a wide range of data (Cavanaugh *et al.*, 2002; Walker *et al.*, 2002; Xing and Heeger, 2001).

The excitation term $E$ is a linear function of the stimuli contrast, while the inhibitory term is a nonlinear combination of $E$. That is, $E_j = Se_{j,s}C_s + Se_{j,t}C_s$ and $I_j = Si_j C_s^q$. The derivation is detailed in the Appendix.

In our experiment, when the appearance of the test region matches that of the matching region, the responses produced by these two patterns should be the same. Hence,

$$(Ke_m \cdot E_{j\cdot m}^p)/(Ki_m \cdot I_{j\cdot m} + Z) = (Ke_t \cdot E_{j\cdot t}^p)/(Ki_t \cdot I_{j\cdot t} + Z), \tag{3}$$

where the subscripts $m$ and $t$ denote that these parameters are for the matching and test regions, respectively.

Equation (3) can be simplified by two approximations. First, in the matching patterns, the scrambled background would produce little, if any, response in the oriented channels and thus would result in a very weak divisive inhibitory signal, $I_m$. Therefore, on the left-hand side of equation (3), the inhibitory term $I_m$ has a negligible effect. Second, in our data, the matched contrast was always much lower than that of the inducing contrast (Figs 3 and 4). Therefore, for any measurable effect, the inducing contrast must be at least several times higher than threshold. On the other hand, at absolute threshold, the additive constant $Z$ can be approximated by $Z = (Se \cdot C_\theta)^p$, where $C_\theta$ is the contrast threshold of the pattern. Since contrast threshold is less than 1, and power is larger than 1, $Z$ is thus negligible compared with $I_t$. Based on the above considerations, equation (3) can be simplified as:

$$\left(Ke_m \cdot E_{j,m}^p\right)/Z = \left(Ke_t \cdot E_{j,t}^p\right)/(Ki_t \cdot I_{j,t}). \tag{4}$$

Given that $E$ and $I$ are functions of contrast $C$, we arrive at:

$$C_m = gC_s^h, \tag{5}$$

where $C_m$ is matched contrast, $C_s$ is surround contrast, and $g$ is the constant. The derivation is detailed in the Appendix.

Equation (5) was the same equation (equation (1)) that we used to fit our data. Thus, the first approximation of the response characteristics of the inducing effect is a power function. In addition, this model also explains why the power factor $h$ did not vary with spatial configuration, but the gain factor $g$ was in our data. The power factor was a property of the visual mechanisms. As long as the input stimuli are processed by the same mechanisms, the visual performances to these stimuli share the same nonlinearity and thus the same power factor. On the other hand, the gain (or sensitivity) factor was determined by the correspondence between the receptive field structure and the input stimuli, and thus would change with spatial configuration.

### 4.3. Comparison with Previous Studies

In the brightness domain, Howe (2005) showed that the brightness shift of a gray patch when embedded in a high contrast grating (i.e., the White effect) was the same as the shift of a gray patch embedded in a concentric annuli pattern. This is consistent with our results. In addition, we showed that such results can be extended for inducers across a wide range of luminance contrasts and across different isoluminant chromatic modulations.

In a series of studies, Monnier and Shevell (2003, 2004; also see Shevell and Monnier, 2005) showed that the appearance of a gray ring embedded in an $S$-cone modulated concentric pattern inducer shifted toward the color of its immediate neighbors and against its non-contiguous neighbors. This result agrees qualitatively with ours as well. Shevell and Monnier (2005) also measured how induced shift changed with inducer contrast and showed that the induced shift increased monotonically with inducer contrast. This is also consistent with our results. However, they made a claim that the magnitude of the shift increased linearly with the inducer contrast. As discussed above, the linear model did not always fit the data in our case. Shevell and Monnier (2005) provided no statistical tests on whether the induced appearance shift indeed increased linearly with inducer contrast. Actually, some of their data (Shevell and Monnier, 2005, Fig. 3) showed a visible nonlinear trend. One possible explanation of the difference between our result and that of Shevell and Monnier (2005) is the different units of contrast used in the two studies. However, the contrast metrics in these two studies actually had a linear relationship for the $S$-cone conditions. In the $\pm S$ condition, the background $L$-, $M$- and $S$-cone excitations were constants and $\Delta L$ and $\Delta M$ were zero. Hence, the cone contrast was reduced to $C_{\mathrm{sp}} = \Delta S/S_0/(3^{0.5})$. Their contrast metric is $C_{\mathrm{ss}} = \Delta S/(L_0 + M_0)$. Thus, the contrast we used is: $C_{\mathrm{sp}} = C_{\mathrm{ss}} \cdot (L_0 + M_0)/S_0 \cdot (3^{0.5})$ where $L_0$ and $M_0$ are $L$- and $M$-cone excitation of their background and $S_0$ is the $S$-cone excitation of our background. Given that neither of these two studies had the background changed in the respective experiments, the two contrast metrics differed only by a multiplicative constant. Therefore, the difference in the contrast unit cannot explain the difference in the data.

### 4.4. Alternative Explanations

The similarity between the induction effects obtained with the grating and with the concentric annuli inducers may have challenged some current theories on the mechanisms underlying the Munker–White effect. For example, some researchers have suggested that the existence of T-junctions might be essential to explaining the White effect (e.g., Anderson, 1997; Gilchrist *et al.*, 1999). A T-junction refers to the image feature that the end of one line segment contacts with the middle of the other line segment. In the Munker–White effect, T-junctions occur when an observer places a rectangular gray test patch on a black or a white stripe. As suggested, the T-junctions are essential for computing surface properties (Adelson, 1993) or belongingness (Gilchrist *et al.*, 1999) in an image, and in turn determine

the lightness of the test patch. However, we showed that the Munker–White effect was similar to the appearance shift produced by a concentric inducer. Since no T-junctions appear in the concentric annuli, a T-junction apparently is not necessary for the appearance shift observed in the Munker–White effect. This conclusion is consistent with Howe's (2005) in the brightness domain. In addition, Anstis (2005) also observed brightness shifts with a randomly textured inducer and concluded that T-junctions are not a necessary condition for brightness induction. Taken together with our results, T-junctions appear to be unnecessary in the Munker–White effect.

Blakeslee and McCourt (1999) showed that an ODOG (oriented difference-of-Gaussians) multi-scale spatial filtering model predicts the White effect. In their model, a band of linear filters are tuned to different spatial frequencies and orientations. The response of each filter to an input image is normalized such that the RMSE of the filters in each orientation is the same. Their model can predict the White effect because the existence of the test patch provides contrast energy orthogonal to the orientation of the grating inducer. Such contrast energy is augmented during normalization. As a result, the test patch appears brighter when it is superimposed on a dark bar and becomes darker when it is superimposed on a white bar. However, their model cannot predict brightness induction with concentric patterns. If the size of the linear filter is sufficiently large, the linear filters tuned to different orientations have the same response to the concentric patterns. In other words, no RMSE difference exists among filters tuned to different orientations and, in turn, no normalization occurs. Consequently, the operation of this model is simply to decompose the image and recombine it again. In this way, such operation cannot predict brightness shift of a test ring in the concentric annuli. For the ODOG model to work for the concentric annuli, the size of the filters and the spatial extent of the normalization regions have to be small enough to allow the filters to pick up the inhomogeneity in the local orientation information.

## 5. Conclusion

In conclusion, we showed that the appearance shift of the gray test patch induced by a grating surround was quite similar to that induced by a concentric annuli inducer. The appearance shift increased as a power function of inducer contrast for both grating and concentric inducers. The exponent in the power function depended on chromatic modulation and not on spatial configuration of the inducer. This implies that the mechanisms underlying the Munker–White effect and the annulus pattern induction effect share similar nonlinear properties. Such result can be explained by a sensitivity modulation model of lateral interactions.

*Acknowledgement*

This study was supported by National Science Council of Taiwan Grants # 95-2413-H-002-001 and # 96-2413-H-002-006-MY3 to CCC.

## References


Adelson, E. H. (1993). Perceptual organization and the judgment of brightness, *Science* **262**, 2042–2044.

Anderson, B. L. (1997). A theory of illusory lightness and transparency in monocular and binocular images: the role of contour junctions, *Perception* **26**, 419–453.

Anstis, S. M. (2005). White's effect in lightness, color, and motion, in: *Seeing Spatial Form*, L. Harris and M. Jenkin (Eds), pp. 91–99. Oxford University Press, Oxford, UK.

Anstis, S. M. and Cavanagh, P. (1983). A minimum motion technique for judging equiluminance, in: *Colour Vision: Psychophysics and Physiology*, J. D. Mollon and L. T. Sharpe (Eds), pp. 155–166. Academic Press, London, UK.

Blakeslee, B. and McCourt, M. E. (1999). A multiscale spatial filtering account of the White effect, simultaneous brightness contrast and grating induction, *Vision Research* **39**, 4361–4377.

Brainard, D. H. (1997). The psychophysics toolbox, *Spatial Vision* **10**, 433–436.

Carney, T., Tyler, C. W., Watson, A. B., Makous, W., Beutter, B., Chen, C. C. and Norcia, A. M. (2000). Modelfest: first year results and plans for future years, *SPIE Proc.* **3959**, 140–151.

Cavanaugh, J. R., Bair, W. and Movshon, J. A. (2002). Nature and interaction of signals from the receptive field center and surround in macaque V1 neurons, *J. Neurophysiol.* **88**, 2530–2546.

Chen, C. C. and Foley, J. M. (2004). Pattern detection: interactions between oriented and concentric patterns, *Vision Research* **44**, 915–924.

Chen, C. C. and Tyler, C. W. (1999). Spatial pattern summation is phase-insensitive in the fovea but not in the periphery, *Spatial Vision* **12**, 267–285.

Chen, C. C. and Tyler, C. W. (2001). Lateral sensitivity modulation explains the flanker effect in contrast discrimination, *Proc. Royal Soc. B: Biol. Sci.* **268**, 509–516.

Chen, C. C. and Tyler, C. W. (2002). Lateral modulation of contrast discrimination: flanker orientation effects, *J. Vision* **2**, 520–530.

Chen, C. C. and Tyler, C. W. (2008). Excitatory and inhibitory interaction fields of flankers revealed by contrast-masking functions, *J. Vision* **8**, 1–14.

Chen, C. C., Foley, J. M. and Brainard, D. H. (2000). Detection of chromoluminance patterns on chromoluminance pedestals. I: Threshold measurements, *Vision Research* **40**, 773–788.

Chen, C. C., Kasamatsu, T., Polat, U. and Norcia, A. M. (2001). Contrast response characteristics of long-range lateral interactions in cat striate cortex, *Neuroreport* **12**, 655–661.

Daugman, J. G. (1980). Two-dimensional spectral analysis of cortical receptive field profiles, *Vision Research* **20**, 847–856.

DeMarco, P., Pokorny, J. and Smith, V. C. (1992). Full-spectrum cone sensitivity functions for X-chromosome-linked anomalous trichromats, *J. Optic. Soc. Amer.* **9**, 1465–1476.

Foley, J. M. (1994). Human luminance pattern–vision mechanisms: masking experiments require a new model, *J. Optic. Soc. Amer. A: Optics, Image Sci., Vision* **11**, 1710–1719.

Foley, J. M. and Chen, C. C. (1999). Pattern detection in the presence of maskers that differ in spatial phase and temporal offset: threshold measurements and a model, *Vision Research* **39**, 3855–3872.

Freeman, W. T. and Adelson, E. H. (1991). The design and use of steerable filters, *IEEE Trans. Pattern Anal. Machine Intell.* **13**, 891–906.

Gilchrist, A., Kossyfidis, C., Bonato, F., Agostini, T., Cataliotti, J., Li, X., Spehar, B., Annan, V. and Economou, E. (1999). An anchoring theory of lightness perception, *Psychol. Rev.* **106**, 795–834.

Heeger, D. J. (1992). Normalization of cell responses in cat striate cortex, *Visual Neurosci.* **9**, 181–197.

Hong, S. W. and Shevell, S. K. (2004). Brightness contrast and assimilation from patterned inducing backgrounds, *Vision Research* **44**, 35–43.

Howe, P. D. L. (2005). White's effect: removing the junctions but preserving the strength of the illusion, *Perception* **34**, 557–564.

Hubel, D. and Wiesel, T. N. (1962). Receptive fields, binocular interaction and functional architecture in the cat's visual cortex, *J. Physiol.* **160**, 106–154.

Kelly, D. H. (1983). Spatiotemporal variation of chromatic and achromatic contrast thresholds, *J. Optic. Soc. Amer.* **73**, 742–750.

Legge, G. E. and Foley, J. M. (1980). Contrast masking in human vision, *J. Optic. Soc. Amer.* **70**, 1458–1471.

MathWorks (1993). *MATLAB*. The MathWorks Inc., Natick, Massachusetts, USA.

Monnier, P. (2008). Standard definitions of chromatic induction fail to describe induction with S-cone patterned backgrounds, *Vision Research* **48**, 2708–2714.

Monnier, P. and Shevell, S. K. (2003). Large shifts in color appearance from patterned chromatic backgrounds, *Nature Neurosci.* **6**, 801–802.

Monnier, P. and Shevell, S. K. (2004). Chromatic induction from S-cone patterns, *Vision Research* **44**, 849–856.

Mullen, K. T. (1985). The contrast sensitivity of human colour vision to red–green and blue–yellow chromatic gratings, *J. Physiol.* **359**, 381–400.

Munker, H. (1970). *Farbige Gitter, Abbildung auf der Netzhaut und ubertragungstheoretische Beschreibung der Farbwahrnehmung*. Habilitationsschrift, Munchen, Germany.

Pelli, D. G. (1997). The VideoToolbox software for visual psychophysics: transforming numbers into movies, *Spatial Vision* **10**, 437–442.

Polat, U., Mizobe, K., Pettet, M. W., Kasamatsu, T. and Norcia, A. M. (1998). Collinear stimuli regulate visual responses depending on cell's contrast threshold, *Nature* **391**, 580–584.

Robson, J. G. (1966). Spatial and temporal contrast-sensitivity functions of the visual system, *J. Optic. Soc. Amer.* **56**, 1141–1142.

Ross, J. and Speed, H. D. (1991). Contrast adaptation and contrast masking in human vision, *Proc. Royal Soc. B: Biol. Sci.* **246**, 61–69.

Shevell, S. K. and Monnier, P. (2005). Color shifts from S-cone patterned backgrounds: contrast sensitivity and spatial frequency selectivity, *Vision Research* **45**, 1147–1154.

Smith, V. C. and Pokorny, J. (1975). Spectral sensitivity of the foveal cone photopigments between 400 and 500 nm, *Vision Research* **15**, 161–171.

Stork, D. G. and Wilson, H. R. (1990). Do Gabor functions provide appropriate descriptions of visual cortical receptive fields? *J. Optic. Soc. Amer. A* **7**, 1362–1373.

Taya, R., Ehrenstein, W. H. and Cavonius, C. R. (1995). Varying the strength of the Munker–White effect by stereoscopic viewing, *Perception* **24**, 685–694.

Teo, P. C. and Heeger, D. J. (1994). Perceptual image distortion, *SPIE Proc.* **2179**, 127–141.

Tyler, C. W. and McBride, B. (1997). The Morphonome image psychophysics software and a calibrator for Macintosh systems, *Spatial Vision* **10**, 479–484.

Vos, J. J. (1978). Colorimetric and photometric properties of a 2-deg fundamental observer, *Color Res. Appl.* **3**, 125–128.

Walker, G. A., Ohzawa, I. and Freeman, R. D. (2002). Disinhibition outside receptive fields in the visual cortex, *J. Neurosci.* **22**, 5659–5668.

Watson, A. B. and Solomon, J. A. (1997). A model of visual contrast gain control and pattern masking, *J. Optic. Soc. Amer. A* **14**, 2378–2390.

Watson, A. B., Barlow, H. B. and Robson, J. G. (1983). What does the eye see best? *Nature* **302**, 419–422.

White, M. (1979). A new effect of pattern on perceived lightness, *Perception* **8**, 413–416.

White, M. (1981). The effect of the nature of the surround on the perceived lightness of grey bars within square-wave test gratings, *Perception* **10**, 215–230.

Wilson, H. R. and Humanski, R. (1993). Spatial frequency adaptation and contrast gain control, *Vision Research* **33**, 1133–1149.

Xing, J. and Heeger, D. J. (2001). Measurement and modeling of center-surround suppression and enhancement, *Vision Research* **41**, 571–583.

## Appendix

The excitation $E_j$ is determined by the cross-correlation between the sensitivity profile and the image. In our study, the inducing pattern contains a square-wave inducer and a test region. The test region can be considered as a rectangular function added to the square wave. We assume that the sensitivity profile of the mechanism is similar to the receptive field of a simple cell in the primary visual cortex (Hubel and Wiesel, 1962) and thus can be described by a Gabor function (Daugman, 1980) or other types of wavelets (Freeman and Adelson, 1991; Heeger, 1992; Stork and Wilson, 1990). The excitatory input to the response function is then:

$$\begin{aligned} E_j &= \sum_{x,y} f_j(x,y) \cdot (h_s(x,y) + h_t(x,y)) \\ &= \left[ \sum_{x,y \in s^+} f_j(x,y) \cdot (C_s \cdot L_0) - \sum_{x,y \in s^-} f_j(x,y) \cdot (C_s \cdot L_0) \right] \\ &\quad + \alpha \cdot \sum_{x,y \in t} f_j(x,y) \cdot (C_s \cdot L_0) \\ &= Se_{j,s} C_s + Se_{j,t} C_s \\ &= E_{j,s} + E_{j,t}, \end{aligned} \tag{A.1}$$

where $f_j$ is the spatial sensitivity profile of the filter; subscript $t$ indicates the test region; subscript $s$ indicates the inducer region; subscripts $s^+$ and $s^-$ indicate the brighter and darker parts of the inducer region, respectively; $C_s$ is the inducer contrast; and $L_0$ is the mean luminance. The parameter $\alpha$ is 1 if the test region was superimposed on the darker bar (Munker–White) or ring (annulus pattern induction) of the inducer and $-1$ if superimposed on the brighter bar or ring. The excitation of the $j$th mechanism to an image component is thus the product of the inducer contrast $C_s$ and a sensitivity constant $Se_{j,s}$ or $Se_{j,t}$, respectively, for the inducer and the target, determined by the spatial profile of the filter and the corresponding image component. The excitation to the matching pattern can be derived in a similar fashion as $E_{j,b} + E_{j,m}$ where $E_{j,b} = Se_{j,b} C_s$ is the excitation to the scrambled binary background, and $E_{j,m} = Se_{j,b} C_m$ is the excitation to the matching region, where $C_m$ is the matching contrast. Here, we used the properties that the product of a wavelet and a periodic pattern summed over space can be described by a product of the pattern contrast and a constant.

The inhibitory input is a nonlinear combination of the rectified excitations of all the filters centered at the same location, over all orientations and phases (Chen and Foley, 2004). Thus, the inhibition input for the $j$th mechanism is:

$$I_j = \sum_n w_n E_n^q = Si_j C_s^q, \tag{A.2}$$

where $w_n$ are weights, $q$ is the power factor, and $Si_j = {}_n[w_n(Se_{n,s} + Se_{n,t})^q]$ is the sensitivity of the $j$th mechanism to the divisive inhibition input.

In equation (5), the constant $g$ equals $[Ke_t \cdot Z \cdot (Se_{j,s} + Se_{j,t})^p]/Ke_m \cdot Ki_t \cdot Se_{j,m}^p \cdot Si_{j,t}^q$, which contains all the sensitivity terms and can be regarded as the gain factor for the inducer, and $h = p - q$ is the power factor, which was related to the nonlinearity in the system.